Sensors and Materials, Vol. 38, No. 1 (2026) 265–276
MYU Tokyo

S & M 4298

Assessment of Coastal Erosion Vulnerability Using Aerial Sensing and Geospatial Data

Yong Huh[1] and JaeKang Lee[2*]

[1]Planning and Coordination Office, Korea Research Institute for Human Settlements,
5 Gukchaegyeonguwon-ro, Sejong-si 30147, Republic of Korea
[2]Department of Civil Engineering, Dong-A University,
32, Daesingongwon-ro, Seo-gu, Busan 49201, Republic of Korea

(Received November 7, 2025; accepted December 5, 2025)

Keywords: coastal area, erosion vulnerability, geospatial data, digital twin

Coastal erosion vulnerability assessments are critical for planning effective coastal defense; however, previous methods that rely on low-resolution data often lack the analytical precision required for local- or site-specific coastal management. This study presents an improved approach that constructs a 3D geospatial digital twin of coastal areas by integrating high-resolution aerial image data and topo-bathymetric light detection and ranging (Lidar) data, which are acquired by airborne sensors. Using this digital twin, coastal erosion vulnerability was assessed at 5 m intervals along the coastline in the digital twin based on six vulnerability indices including geomorphological feature, beach width, coastal slope, and so on. A key innovation of the proposed method is the application of the Jenks natural breaks optimization to measure vulnerability scores for each index. Then, the vulnerability assessment is determined by combining these six scores. The method was applied to a coastal area in Uljin-gun, Republic of Korea, and, unlike previous low-resolution 2D data assessment approaches, it successfully identified specific coastline segments exhibiting high vulnerability that would not be identified with previous approaches.

1. Introduction

Coastal erosion breaks down rocks, soil, and sand along coasts through local sea level rise, strong wave action, and coastal flooding. It is a critical problem because many development activities such as residential development, industrial development, transportation, and tourism are common in coastal areas. To address this problem, recent geospatial data and techniques have been used to study coastal erosion. In previous studies, various analyses related to coastal management were conducted by modeling the terrain of the coastal area using 3D geospatial information.[1,2] Moreover, several studies[3–5] presented an approach for coastal management utilizing high-precision geospatial information, which was acquired using optical cameras mounted on unmanned aerial vehicles or using light detection and ranging (Lidar) equipment. Accordingly, a

*Corresponding author: e-mail: spinsgis@gmail.com
https://doi.org/10.18494/SAM6004

ISSN 0914-4935
https://myukk.org/

vulnerability assessment model was developed by integrating these research findings on the spatial information and analysis models for coastal areas.[6,7]

With the recent development of geospatial information technology, accurate aerial images and Lidar data can be acquired simultaneously, and a large amount of data can be processed and analyzed effectively. The European Union developed Destination Earth, which includes high-precision digital models of the Earth that integrate various aspects of the Earth's system to monitor and simulate natural phenomena and related human activities.[8] Moreover, Duque and Brovelli[8] suggested a plan to build an integrated geospatial dataset for the Italian coast. Allen *et al.*[9] proposed a digital twin system structure and a service that provides conditional decision-making to analyze and predict floods in coastal areas.

In the vulnerability assessment model, several previous studies have utilized geospatial data with a low spatial resolution instead of precise large-scale geospatial information acquired through the latest geospatial technologies, resulting in inaccuracy for small-scale vulnerability assessment. For example, small rocks distributed locally in many coastal areas can be erroneously detected as erosion prevention facilities. Conversely, ground erosion may occur even on rocky coasts where roads or buildings are located and on locally distributed sand dunes, which can contribute to sinkholes. Although several studies[3–5] suggested methods for constructing more precise 2D or 3D geospatial information, information on the land cover condition was not comprehensively analyzed or utilized through aerial image or Lidar data analysis.

To address this gap, we propose a method to assess vulnerability to coastal erosion with a 3D geospatial dataset using the latest geospatial information technology. On the basis of this dataset, a 3D virtual representation of the area was obtained, which can implement a detailed vulnerability assessment to predict small-scale erosions and plan appropriate coastal structures. In the 3D virtual representation, namely, the Digital Twin, various spatial criteria used for vulnerability analysis in previous studies were measured along the coastline at specific intervals, and each was normalized to a range between 0 and 1. Then, Jenks natural breaks optimization[10–12] was applied to the normalized values for each spatial criterion to perform clustering, and the value of one spatial criterion for the segment in the cluster was simplified to the ranking score of the cluster. Given a specific interval along the coastline, the simplified scores of each criterion are then processed to obtain a single coastal vulnerability score (*CVC*). After calculating the scores for all segments in this manner, the vulnerability indices were then determined by applying the Jenks natural breaks optimization once again. The specific data, methodology, and experimental results are as follows.

2. Data and Methods

2.1 Study area and geospatial data

The proposed dataset and assessment method were applied to a coastal area located in Uljin-gun, Republic of Korea, as shown in Fig. 1. Three types of geospatial data were used to

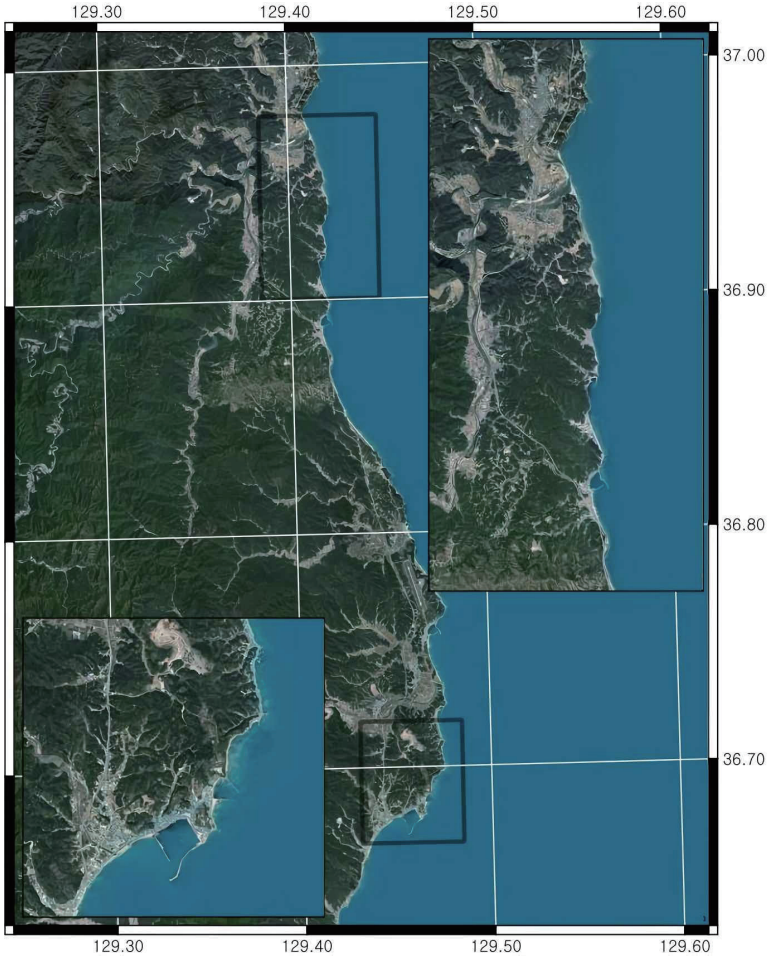

Fig. 1. (Color online) Location of study areas in Uljin-gun, Republic of Korea.

construct a 3D integrated geospatial dataset. Among them, aerial image data and point cloud data were acquired using Leica DMC III and Chiroptera 4×, as shown in Table 1. Data on facilities and buildings were extracted from the datasets provided by the government-operated National Spatial Data Infrastructure Portal. Additionally, the linear geospatial data extracted from the coastal management database of the National Spatial Data Infrastructure Portal were used to obtain the required coastline data for the proposed analysis method. Figure 2 shows the geospatial data of the study area.

2.2 Methods

The *CVC* was determined by applying six criteria using Eq. (1):

$$CVC = \sqrt{a \cdot b \cdot c \cdot d \cdot e \cdot f}\,. \tag{1}$$

Table 1
Specifications of data acquisition instruments.

Camera/Lidar instrument		GPS/INS instrument	
Camera model	DMC III	GPS model	AT1675-80
Focal length	92 mm	GPS std	0.05 m
Spatial resolution	8 cm	INS model	LCI-100C
Lidar model	Leica Chiroptera 4X	INS std	0.01 deg
Lidar depth range	2.7 /k		

k : diffuse attenuation coefficient

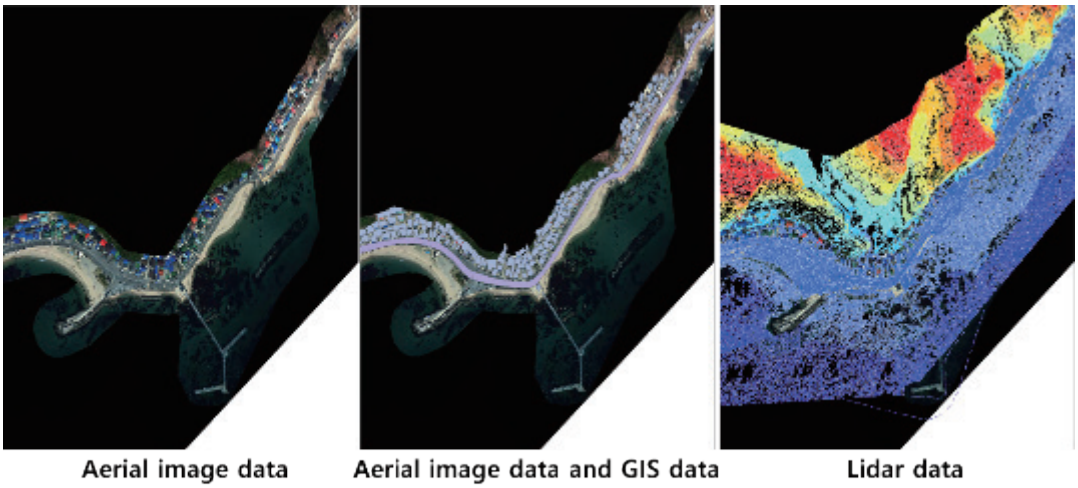

Fig. 2. (Color online) Geospatial data (partial) of the study area.

The four criteria [(a)–(d)] were related to the geospatial information obtained from aerial images, which were acquired using the instruments listed in Table 1. Criteria (e) and (f) were obtained on the basis of the information on the facilities and buildings in the study area, which were managed by public institutions. Since each criterion has a different range of values, normalization is necessary. However, performing simple min-max normalization can lead to distortion caused by some outliers (over- or underestimated observations). Specifically, if the observations are likely to form several clusters related to vulnerability, applying min-max normalization including outliers can result in clusters with different characteristics having similar normalized values. Therefore, in this study, we extracted clusters from the observations and assigned a score of $1/n$ to the cluster with the lowest erosion risk, followed by scores of $2/n$, $3/n$, $4/n$, etc., where n is the number of these clusters in order of increasing risk. These clusters are calculated using the Jenks natural breaks algorithm. Details of the six criteria are as follows.

2.2.1 Geomorphology

The coastal geomorphology can be classified into rock, dune (sand), mudflat, and waterbody. The erosion risk was assessed according to the size and distribution of rocks located on the water surface, which can break the waterflow. Thus, extracting geomorphic features and rocks from

aerial images is necessary.[13–15] In this study, eCognition Developer 9.1, an image processing software program, was used to extract terrain and rock objects, as shown in Fig. 3, according to the multiresolution segmentation.[16] Then, a 10-m-long rectangular area toward the sea was calculated for each interval along the coastline, and the area ratio of rock extracted from the imagery was calculated for every coastline interval. For the area ratio values, the Jenks natural breaks algorithm was applied. The cluster with the highest mean ratio was identified as the lowest erosion risk, so that the coast intervals have a score of 1/*n*. Then, the intervals of the cluster with the second value have a score of 2/*n* and so on, where n is the number of clusters. The same method is applied to the remaining criteria.

2.2.2 Beach width

A beach acts as a barrier and dissipates wave energy; particularly, beaches with large widths reduce not only the wave magnitude considerably but also the impacts of extreme weather events.[17] Therefore, the larger the beach width, the greater the coastal erosion that can be prevented. Beach width was calculated by measuring the width of the dune (sand) terrain object extracted along the coast, as shown in Fig. 3.

2.2.3 Regional elevation

High-elevation coastal regions are considered less vulnerable because they provide higher resistance to inundation against rising sea levels, tsunami run-ups, and storm surges.[17] In this

(a) (b)

Fig. 3. (Color online) Aerial images of the (a) study area and (b) feature objects extracted from the image using eCognition Developer 9.1.

study, the risk level increased as the elevation decreased. The regional elevation values were obtained by constructing a digital elevation model (DEM) from Lidar data using the geographical information system software ArcMap 10.8, with a spatial resolution of 5 m; subsequently, the coastline data extracted from the coastal management database of the National Spatial Data Infrastructure Portal were overlapped on the DEM. The risk level was determined according to the criteria described above.

2.2.4 Coastal slope

The coastal slope is defined as the ratio of the altitude change to its horizontal distance within two points on the coast. A gentle coastal slope has greater penetration of seawater towards the land, whereas coasts with a high slope have less seawater penetration because of wave energy dissipation.[16] In this study, the coastal slope was obtained by constructing a DEM with a spatial resolution of 5 m for bathymetry, similar to that used for calculating the regional elevation.

2.2.5 Defense facility

The study area is characterized by the proximity of mountains and the coast, with roads and residential facilities developed around the coast. Accordingly, various erosion defense facilities are installed in this region to prevent coastal erosion. Compared with natural coasts, an artificial coast with installed facilities should exhibit a low risk. According to the coastal management DB provided by the National Spatial Data Infrastructure Portal, coastlines are divided into natural and artificial coasts, and erosion prevention facilities are observed as polygonal (polygon) objects. In this study, the value of artificial coasts was assigned as 0.2, whereas the value of natural ones as 1.

2.2.6 Distance to town and road

Determining the criterion for the impact of coastal erosion on buildings or roads is difficult. Thus, more rigorous management is necessary for coastal areas adjacent to buildings or roads, even under the same risk level. The *CVC* was also applied to analyze the priorities for such management efforts. Therefore, the risk level was determined to adjust the *CVC* to a higher level as the buildings or roads were closer to the coast.3.

3. Results

Figure 4 shows the 3D high-precision digital twin space in the coastal area, constructed using the geospatial information technology described in Table 1. Geomorphology and beach width were measured by applying automated image analysis technology to aerial image data, and the regional elevation of the ground and the coastal slope below sea level were obtained from Lidar data, as shown in Fig. 5.

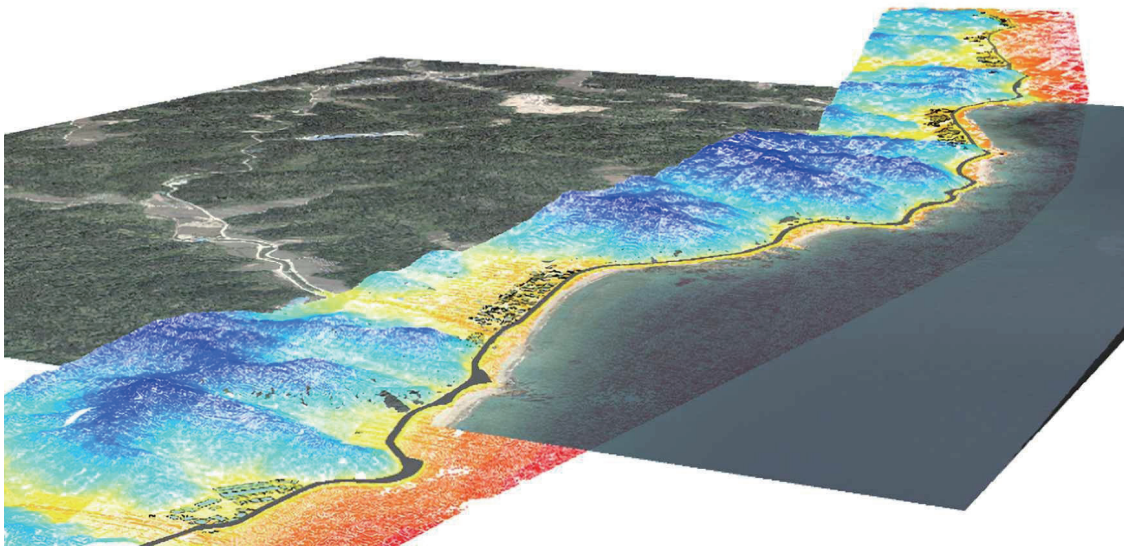

Fig. 4. (Color online) Digital twin (partial) built using geospatial information database of coastal area management agency, aerial image data, and Lidar data as described in Table 1.

In the study area, the percentage of the sand dune or beach coasts was the highest (79.3%), followed by that of the sand dune with small rocks (9.4%). Other terrain types accounted for approximately 6%, and artificial structures, such as ports, were included under the rocky base. Moreover, the coastal beach widths of more than 10 m and less than 50 m comprised about 65% of the coastline. Coasts with a beach width of less than 10 m were mostly found to be rocky bases, ports, or coasts installed with erosion prevention facilities. The coastal elevations of 2.5–5 m and 1–2.5 m accounted for 51.3 and 23.8% of the coastline, respectively. The high percentage of the sand dune or beach coasts (79.6%) showed the characteristics of coasts having a low elevation and gentle boundary with the sea level.

A significant error occurred in the calculation process for coastal slopes when the laser of the Leica Chiroptera 4× used in this study did not sufficiently reach the seabed and did not reflect sufficient intensity. The bathymetry of the East Coast, which is the study area, can be described as having a rapid decrease in water depth compared with other coasts; therefore, the Lidar laser could not reach the seabed occasionally or was scattered owing to high waves and the resulting foam. Consequently, compared with the bathymetry data shown in Fig. 5(c) (regional elevation), the coastal slope information shown in Fig. 5(d) indicates that some data are missing or include errors, rendering the slope information at that point unfeasible. Moreover, 34.1% of the coastline had a slope of 0.1–0.15, whereas 27.3% had a slope of 0.05–0.1. Generally, when the beach width was 50 m or more, the slope was <0.1, representing flat topographical characteristics. As shown on the right side of Fig. 5(a) (geomorphology), in some cases, the slope had a high value when rocks were distributed around the sandy beach.

In the study area, most coastlines were natural coastlines (94.3%), with only 5.7% representing artificial coastlines, such as areas with ports or those installed with erosion prevention facilities. Regarding the distance from buildings and facilities, roads were built all

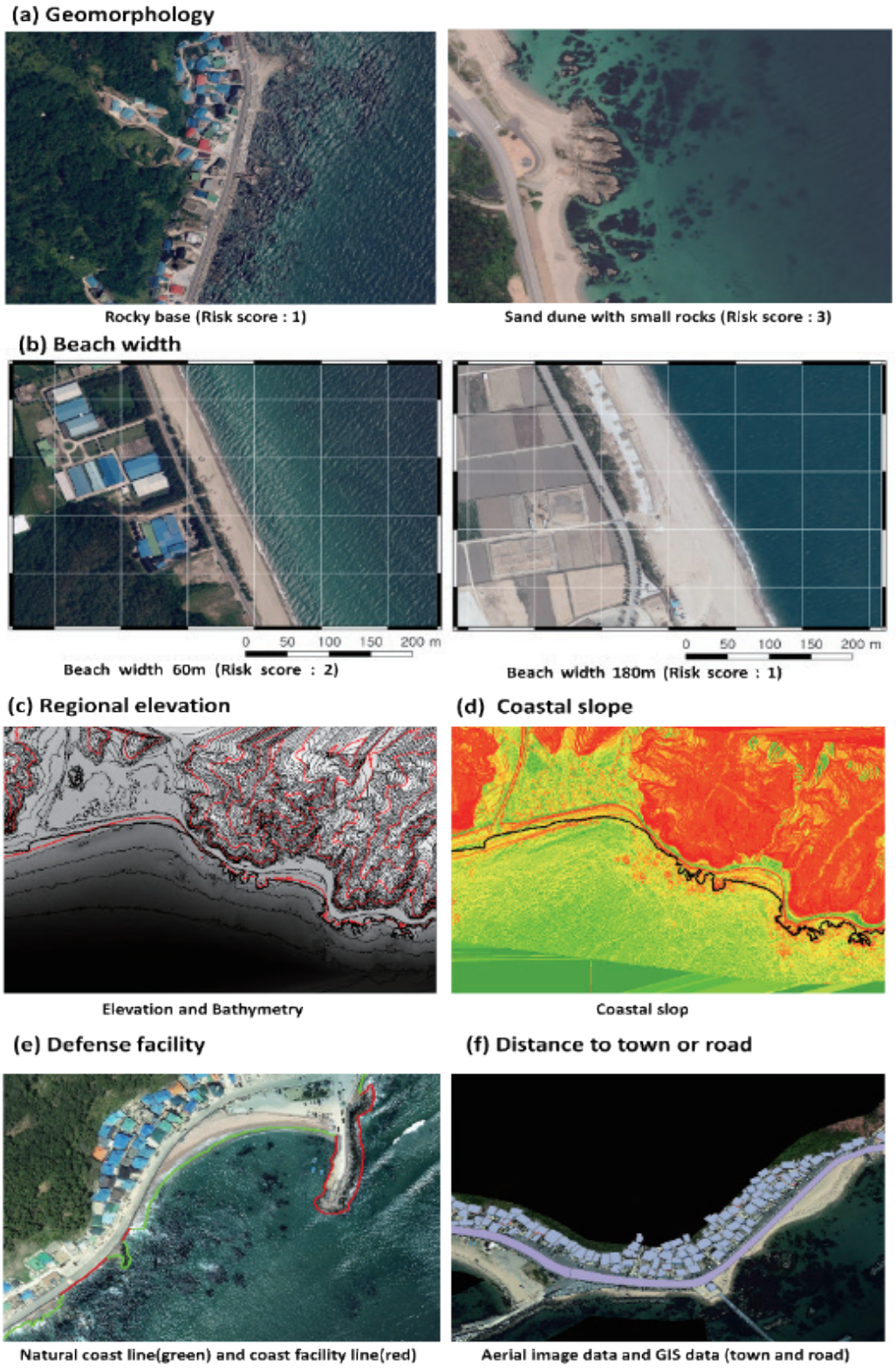

Fig. 5. (Color online) Cases of six criteria in the study area in Fig. 1.

along the coast of the study area. Although the distance between the coasts and some roads was > about 100 m, as shown in Fig. 5(b) (beach width), most roads were within about 25 m from the coast [Fig. 5(a) (geomorphology)].

The *CVC* value can be calculated by applying the acquired six criteria values to Eq. (1). In this study, the coastline was divided into 5 m intervals, and the *CVC* values were calculated for each segment. The corresponding results are shown in Fig. 6. The mid-section of the coastline shown in Fig. 4 represents an area with a beach width of <10 m; moreover, the road was located close to the coast, and the coastal slope was relatively high. Subsequently, the calculated *CVC* value showed a high risk for this section. In contrast, under the same conditions, the coastline shown in Fig. 6(a) has a local- or site-specific coastal erosion prevention facility, and thus, the risk becomes relatively low. Conversely, the coastline shown in Fig. 6(b), where beach width changes abruptly along the coast, exhibits various *CVC*s as the beach width changes. A small coastline where the sandy beach is much narrower than the surrounding coastline, as indicated by the orange line in Fig. 6(b), can present a high risk of coastal erosion while neighboring coastlines present a low risk. In this case, the proposed method can be utilized to prioritize the deployment of local- or site-specific coastal erosion prevention facilities in high-risk areas and to develop mitigation strategies through the periodic monitoring of the adjacent coastlines.

4. Discussion

In this study, a high-precision 3D geospatial dataset was constructed using the latest geospatial information construction technology to assess the risk of coastal erosion. In previous studies, risk assessments considering the changes in the coastline over the years, sea level rise, and tidal differences were conducted. While many studies have attempted to detect changes in the coastline using aerial images, the detection of such changes arising due to coastal erosion or temporal changes in water level is challenging using only images because the sea level changes

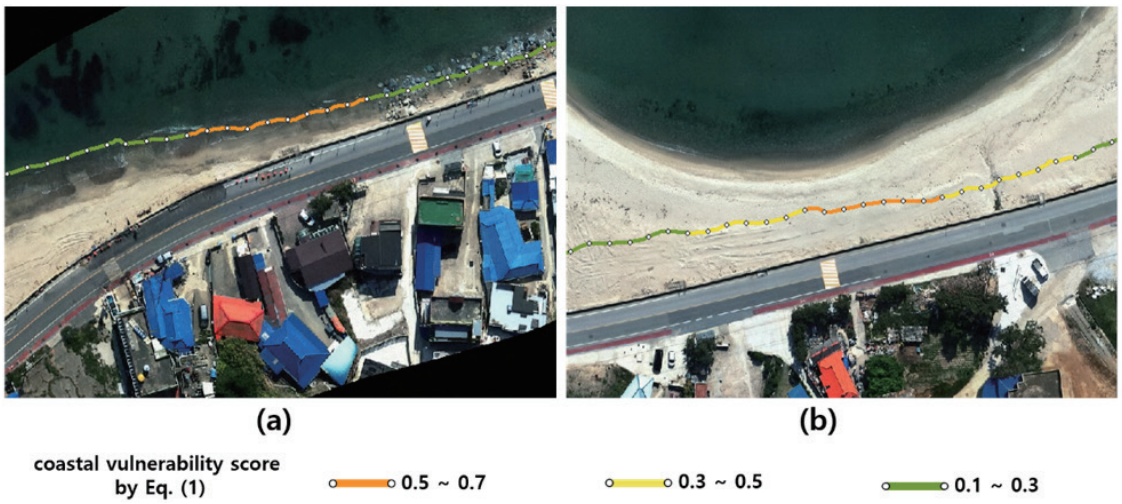

Fig. 6. (Color online) CVC results acquired by the proposed method along the coastline at an interval of 5 m.

according to the image capture time. Compared with previous studies, in this study, coastline changes were analyzed at a high spatial resolution. As reported in previous studies, sea level rise and tidal changes produce effects at regional (tens-to-hundreds km) scales that alter coastal hydrodynamics relevant to erosion.[18] However, as the spatial domain of this study was relatively small (within 20 km), although the effect of sea level rise and tidal differences existed, it appeared to be statistically insignificant. Nevertheless, the analysis based on 3D geospatial information conducted in this study was more precise than that conducted in previous studies. Therefore, analyzing the global *CVC* for a wide domain is appropriate, followed by analyzing the local *CVC* in a higher resolution using the proposed method for maintaining erosion prevention facilities and other purposes.

In this study, in addition to beach width, various geomorphological parameters were extracted by applying image analysis technology to high-resolution aerial images, and the extracted parameters were used for calculating *CVC*. While this approach allowed for more comprehensive analysis using high-resolution data, it also resulted in errors while calculating the coastal slope. Regional elevation and coastal slope were calculated after converting Lidar data into gridded data at 5 m intervals. However, as shown on the right side of Fig. 5(a) (geomorphology), when small-scale rocks were distributed along the coast, the coastal slope was calculated by combining the height values of these rocks on the seafloor terrain where the rocks were distributed. Since the Lidar data were acquired with high-point density, stable results can be obtained when the regional elevation was measured on the ground, with more than 100 height values acquired in a grid space of 5 m × 5 m. However, in the case of bathymetry, the slope was over-measured or under-measured in some cases. This was because less than 20–30 height values were acquired depending on the water quality affected by floating objects or the material characteristics constituting the sea surface, and the bathymetry measured using these height values differed from the actual bathymetry. This problem was caused by the increase in the effect of error values as the grid size decreased while calculating the DEM of the bathymetry to perform spatial analysis. Therefore, future research should focus on the optimal data unit for analysis according to the performance of the surveying equipment. Additionally, a verification process is required to determine whether the risk area identified through the proposed method is truly vulnerable to coastal erosion and whether it poses a risk to the safety of coastal buildings or facilities. Presently, in facility safety management, research is underway to measure cavities in underground spaces, such as sinkholes, cracks in old facilities, and ground stability using ground penetration radar (GPR) sensors. Therefore, to verify and improve the accuracy of the proposed *CVC* model, combining the analysis model proposed in this study with the underground geospatial information of the coastal region explored by the GPR sensors is necessary.

5. Conclusion

In this study, high-precision 3D geospatial information on the coastal area was acquired using the latest spatial information construction technology. Information types were combined to establish a geospatial space to apply various analysis techniques. Six criteria (geomorphology, beach width, regional elevation, coastal slope, defense facility, and distance to town or road)

were selected by referring to the *CVC* models proposed in several previous studies, and five differentiated risk levels were applied to the analysis. The results showed that, unlike previous studies, coastal areas having a high risk of erosion could be detected at a local scale, as the spatial information used in this study had higher accuracy and degree of detail. In contrast, the observation systems for sea level changes and tidal differences provided observation data with a spatial resolution of tens of kilometers; therefore, their application as parameters in analyzing a small area, such as that studied in this research, shows limitations. However, with the recent development of technical standards for combining real-time sensor information centered on spatial information, further improvements in coastal management can be achieved if the precise geospatial dataset established in this study and real-time observation data are combined for integrated analysis and monitoring.

Acknowledgments

This research was supported by a grant titled "Development of the integrated utilization and verification system for the realization of hyper-connected digital land (No. RS-2022-00143804)" funded by the Korea Agency for Infrastructure Technology Advancement.

References

1 I. Hassen, C. Fauchard, R. Antoine, T. Roulland, O. Maquaire, S. Costa, and O. Dugué: Bull. Eng. Geol. Environ. **80** (2021) 1375. https://doi.org/10.1007/s10064-020-01955-z
2 M. G. Magarotto, M. F. Costa, J. A. Tenedório, C. P. Silva, and T. L. M. Pontes: J. Coastal Res. **70** (2014) 479. https://doi.org/10.2112/SI70-081.1
3 V. E. Chapapría, J. S. Peris, and J. S. González-Escrivá: Int. J. Environ. Res. Public Health. **19** (2022) 5457. https://doi.org/10.3390/ijerph19095457
4 S. Devoto, V. Macovaz, M. Mantovani, M. Soldati, and S. Furlani: Remote Sens. **12** (2020) 3566. https://doi.org/10.3390/rs12213566
5 Y. Lin, Y. Cheng, T. Zhou, R. Ravi, S. M. Hasheminasab, J. E. Flatt, C. Troy, and A. Habib: Remote Sens. **11** (2019) 2893. https://doi.org/10.3390/rs11242893
6 M. A. Hoque, N. Ahmed, B. Pradhan, and S. Roy: Ocean Coastal Manage. **181** (2019) 104898. https://doi.org/10.1016/j.ocecoaman.2019.104898
7 K. Nunez, T. Rudnicky, P. Mason, C. Tombleson, and M. Berman: Ecol. Eng. **179** (2022) 106617. https://doi.org/10.1016/j.ecoleng.2022.106617
8 J. P. Duque and M. A. Brovelli: Proc. Int. Archiv. Photogrammetry, Remote Sensing and Spatial Information Sciences XLVIII-4/W1-2022 (ISPRS, 2022) 127–133.
9 T. R. Allen, G. McLeod, H. Richter, and A. Nielsen: Proc. IGARSS 2022-2022 IEEE Int. Geoscience and Remote Sensing Symposium (IGARSS and IEEE, 2022) 4739–4742.
10 R. Y. Meddah, T. Ghodbani, R. Senouci, W. Rabehi, L. Duarte, and A. C. Teodoro: Sustainability **15** (2023) 12838. https://doi.org/10.3390/su151712838
11 R. Gui, W. Song, J. Lv, Y. Lu, H. Liu, T. Feng, and S. Linghu: Remote Sens. **17** (2025) 1092. https://doi.org/10.3390/rs17061092
12 M. M. Islam, D. A. A. Rafi, A. Jannat, K. Aruga, S. Liebenehm, and R. Hossain: J. Coast. Conserv. **29** (2025) 14. https://doi.org/10.1007/s11852-024-01093-8
13 A. Papakonstantinou, K. Topouzelis, and G. Pavlogeorgatos: ISPRS Int. J. Geo-Inf. **5** (2016) 75. https://doi.org/10.3390/ijgi5060075
14 S. Sreekesh, N. Kaur, and S. R. S. Naik: Remote Sens. Earth Syst. Sci. **3** (2020) 24. https://doi.org/10.1007/s41976-020-00032-z
15 A. Zaki, I. Buchori, A. W. Sejati, and Y. Liu: Egypt. J. Remote Sens. Space. Sci. **25** (2022) 349. https://doi.org/10.1016/j.ejrs.2022.03.002

16 K. S. S. Parthasarathy, S. Saravanan, P. C. Deka, and A. Devanantham: ISH J. Hydraul. Eng. **28** (2022) 422. https://doi.org/10.1080/09715010.2020.1753250
17 T. S. Kumar, R. S. Mahendra, S. Nayak, K. Radhakrishnan, and K. C. Sahu: J. Coastal Res. **26** (2010) 523. https://doi.org/10.2112/09-1186.1
18 L. Rose, B. Rohith, and P. K. Bhaskaran: Ocean Eng. **266** (2022) 112691. https://doi.org/10.1016/j.oceaneng.2022.112691